CHAPTER IV
RESULTS AND DISCUSSION

4.1 Benzoxazine Monomer Characterization

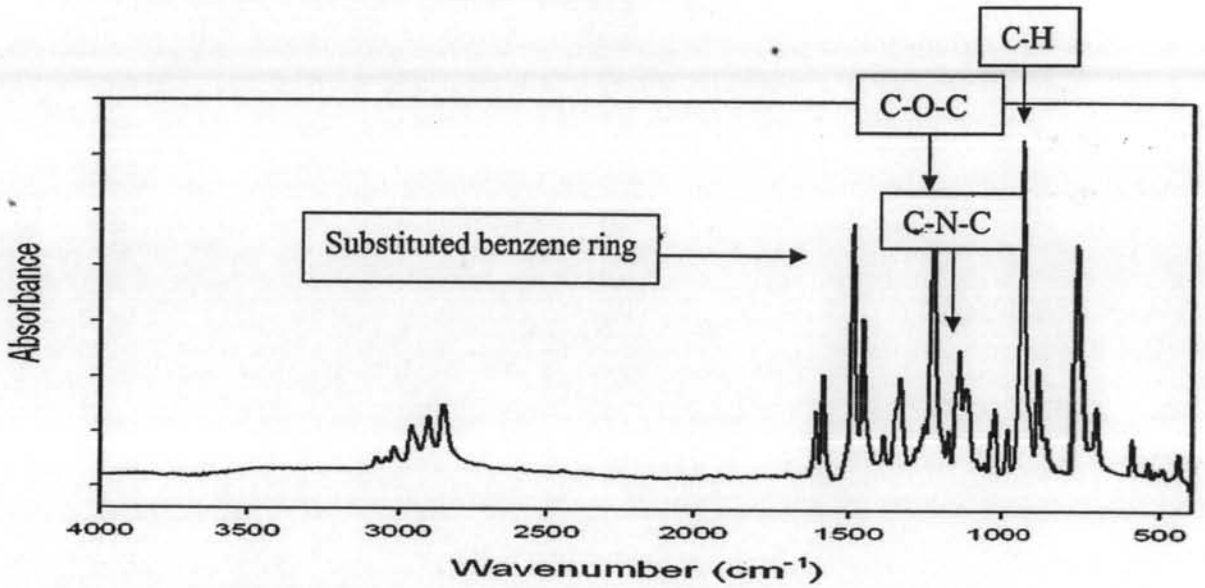

Figure 4.1 FTIR spectra of the diamine-based benzoxazine monomer.

The FTIR spectrum of the bifunctional benzoxazine monomer is shown in Figure 4.1 The bands that appear in the frequency region 1550-1400 cm^{-1} are due to the substituted benzene ring. The bands in the region 1240-1210 cm^{-1} and 1040-1020 cm^{-1} correspond to the antisymmetric and symmetric C-O-C stretching modes. The region of 1150-1050 cm^{-1} is due to the C-N-C antisymmetric stretching, while the symmetric stretching mode appears at 800-720 cm^{-1}. Another characteristic band is the absorption at 918 cm^{-1} which is assigned to the C-H out-of-plane deformation (Ishida, H., and Rodriguez, Y., 1995). Results from gel-permeable chromatography reveal M_n and M_w of benzoxazine monomer are around 1302 and 1454 respectively.

Thermal characterization of the benzoxazine monomer using TGA and DSC are shown in Figure 4.2 and 4.3. TGA experiment results show that benzoxazine monomer started to degrade at 250°C until 800°C with char yield. The DSC thermogram shows that a melting endotherm occurred at 111°C and multiple exotherms occurred at 195°C and 249°C. The exotherm at 195°C might come from the polymerization of benzoxazine monomer to resin The exotherm at 249°C might come from the degradation of benzoxazine monomer, which can also be seen in the TGA experiment, benzoxazine started to degrade at 250°C.

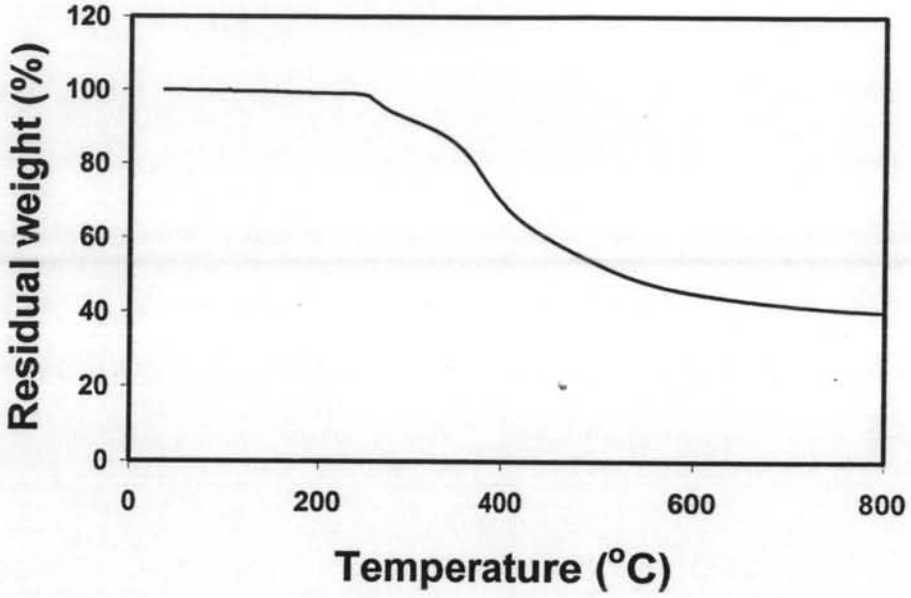

Figure 4.2 TGA thermogram of the diamine-based benzoxazine monomer.

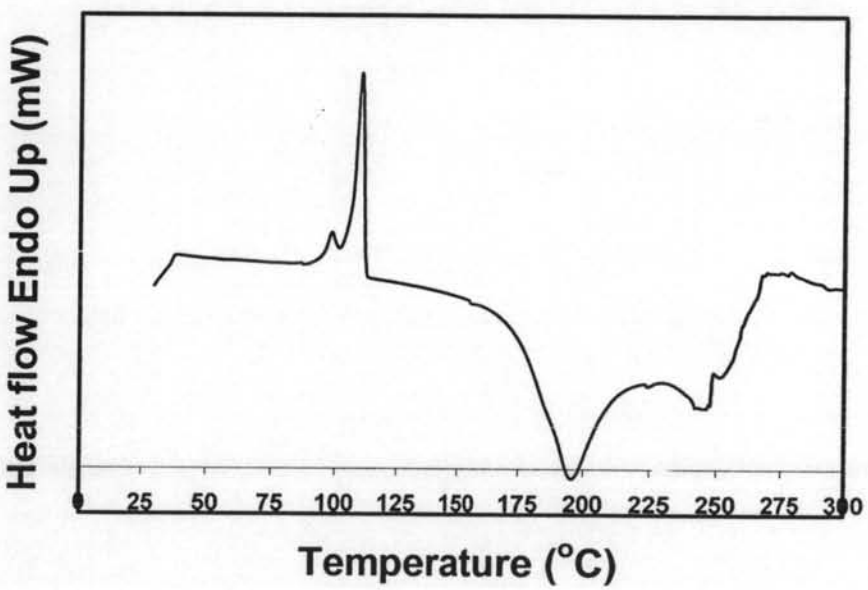

Figure 4.3 DSC thermogram of the diamine-based benzoxazine monomer.

4.2 Barium Titanate/Barium Strontium Titanate Characterization

The crystal phase and structure of barium titanate/barium strontium titanate were measured by XRD. Figure 4.4 (b) shows the XRD spectrum of $BaTiO_3$ from the experiment after the sol-gel process and sintering at 1200°C. It can be seen that the $BaTiO_3$ after the sol-gel has the same crystal phase as the sintered sample and, when compared the positions of both XRD peaks in the experiment are similar to those in XRD patterns (Cho, S.D. et al, 2004). Sharp peaks around 32°, 40°, 45° etc. belong to the perovskite tetragonal phase.

The microstructure and morphology of $BaTiO_3$ after the sol-gel process looks similar to $BaTiO_3$ used in commercial uses, which can be seen in Figure 4.5 (a) and (b). Apparently Figure 4.6 (c) and (d) shows the microstructures of $BaTiO_3$ after sintering at 1200°C, which are not fully sintered at given sintering temperature. It indicates that the sintering temperature should be increased.

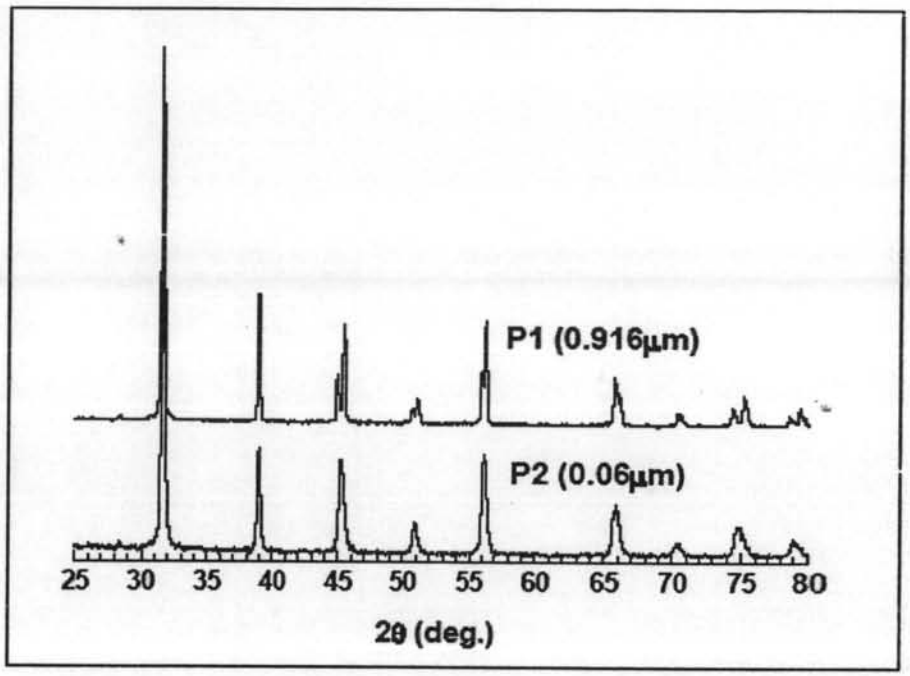

(a)

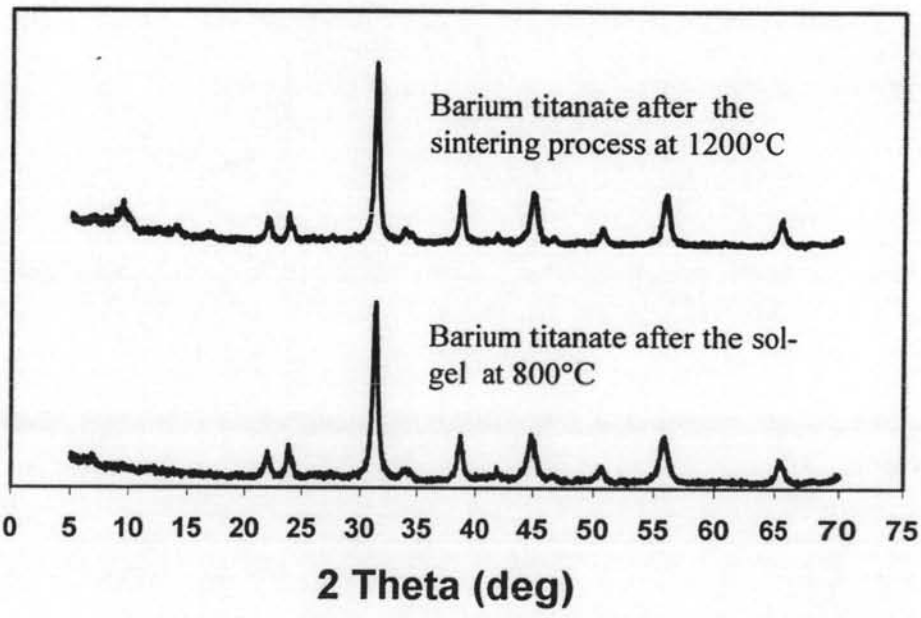

(b)

Figure 4.4 (a) XRD patterns of barium titanate powders at room temperature (reference, Cho, S.D. et al, 2004) and (b) XRD spectrum from experiment of barium titanate after sol-gel and sintering process.

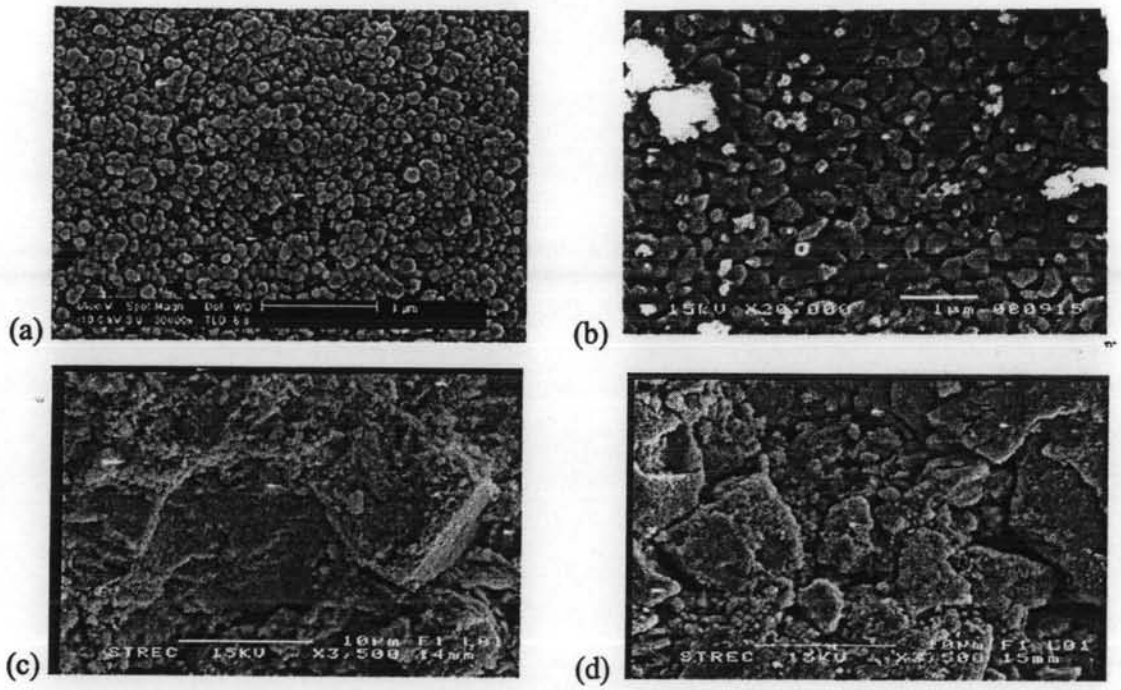

Figure 4.5 SEM images of $BaTiO_3$ (a) reference sol-gel BT powder, (b) after the sol-gel process, (c) and (d) after sintering at 1200°C.

After the content of strontium was increased from 0 to 0.05% by mole, the XRD pattern of the $(Ba_{0.95}Sr_{0.05})TiO_3$ sol-gel powder and sintered product were observed. Figure 4.6 is the XRD spectrum of $(Ba_{0.95}Sr_{0.05})TiO_3$ after the sol-gel and sintering process. It shows that the peaks of $(Ba_{0.95}Sr_{0.05})TiO_3$ after the sol-gel are similar to the peaks of $(Ba_{0.95}Sr_{0.05})TiO_3$ after sintering at 1200°C in positions and intensities and, when compared to those in $BaTiO_3$, it shows that $(Ba_{0.95}Sr_{0.05})TiO_3$ and $BaTiO_3$ still have the same perovskite tetragonal phase. Moreover, the peaks of those two XRD spectrums are also similar to $(Ba_{0.95}Sr_{0.05})TiO_3$ after sintering at 1330°C but the intensity is increased due to the higher sintering temperature which gave a more fully sintered ceramic and higher crystallinity.

Figure 4.7 is the morphology and microstructures of $(Ba_{0.95}Sr_{0.05})TiO_3$. It can be seen that by increasing the sintering temperature, the grain size of $(Ba_{0.95}Sr_{0.05})TiO_3$ is increased because the small particles are fused together to form larger particles at high sintering temperature.

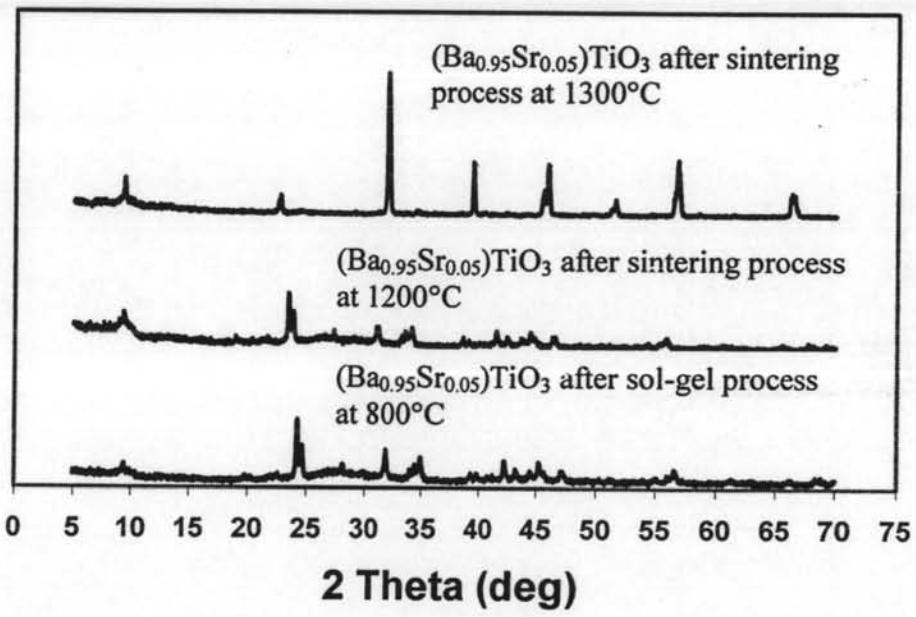

Figure 4.6 XRD spectrum of $(Ba_{0.95}Sr_{0.05})TiO_3$ after sol-gel and sintering process.

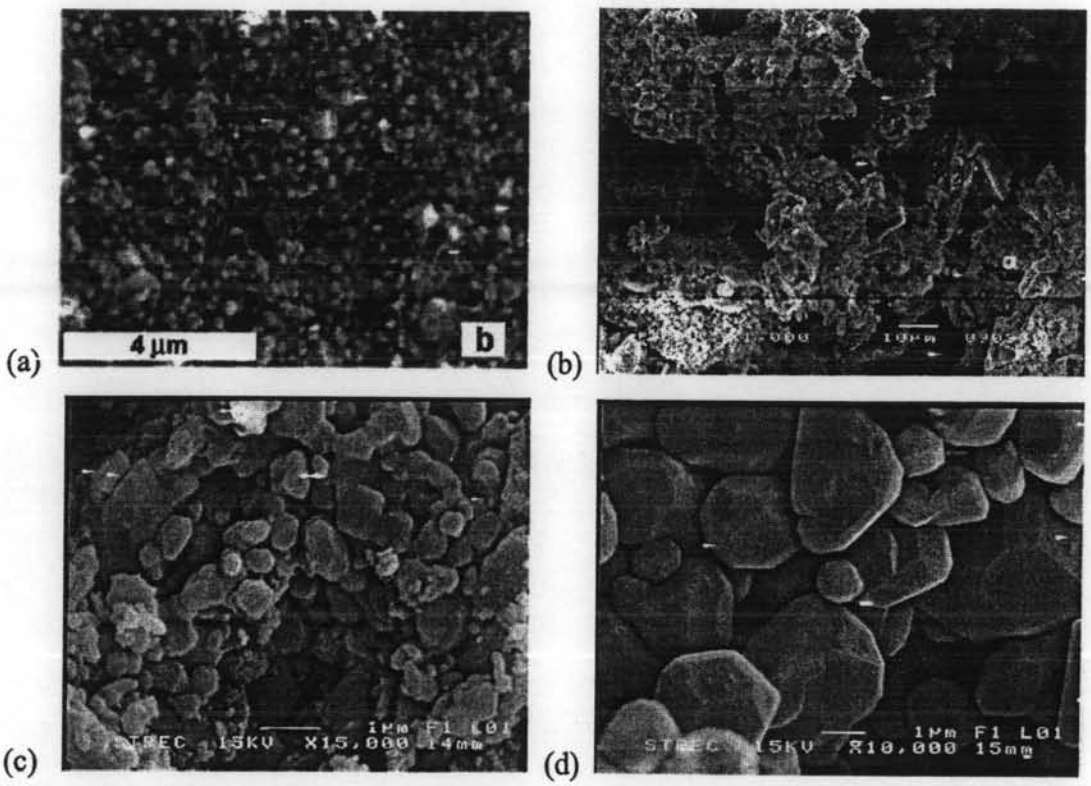

Figure 4.7 SEM images of $(Ba_{0.95}Sr_{0.05})TiO_3$ (a) reference sol-gel BST powder (Hu, T., et al, 2004), (b) after sol-gel process, (c) after sintering at 1200°C, and (d) after sintering at 1330°C.

Figure 4.8 and 4.9 show XRD spectrums of $(Ba_{0.7}Sr_{0.3})TiO_3$ and $(Ba_{0.5}Sr_{0.5})TiO_3$ after the sol-gel process. It shows that when the amount of strontium were increased (from 0.05% to 0.3% and 0.5% by mole), XRD patterns become broaden. It suggests that the structures are not fully crystalline, indicating the temperature of thermal decomposition in sol-gel process is not high enough. By increasing the amount of strontium, the sol-gel process of barium strontium titanate should use higher temperature for thermal decomposition.

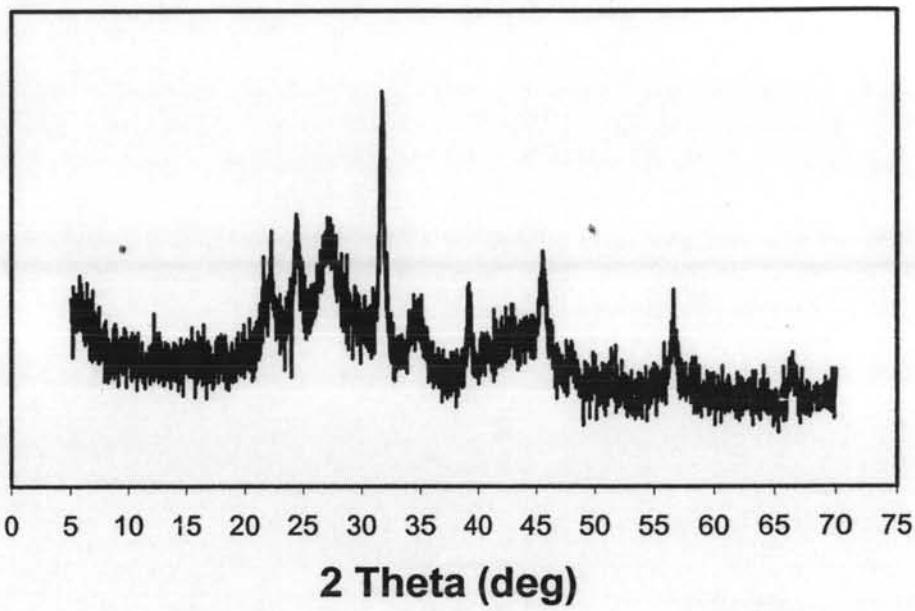

Figure 4.8 XRD spectrum of $(Ba_{0.7}Sr_{0.3})TiO_3$ after sol-gel process.

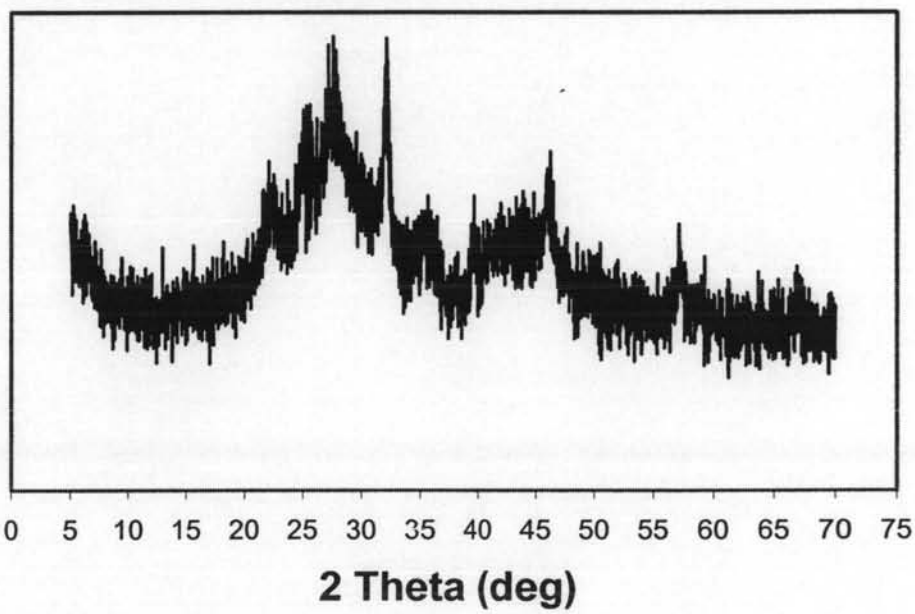

Figure 4.9 XRD spectrum of $(Ba_{0.5}Sr_{0.5})TiO_3$ after sol-gel process.

For $BaTiO_3$, increasing the sintering temperature from 1200°C to 1330°C. XRD patterns in Figure 4.10 shows that the higher temperature in sintering process makes fully crystalline which can be seen from all major peaks. These patterns are corresponding to perovskite tetragonal phase.

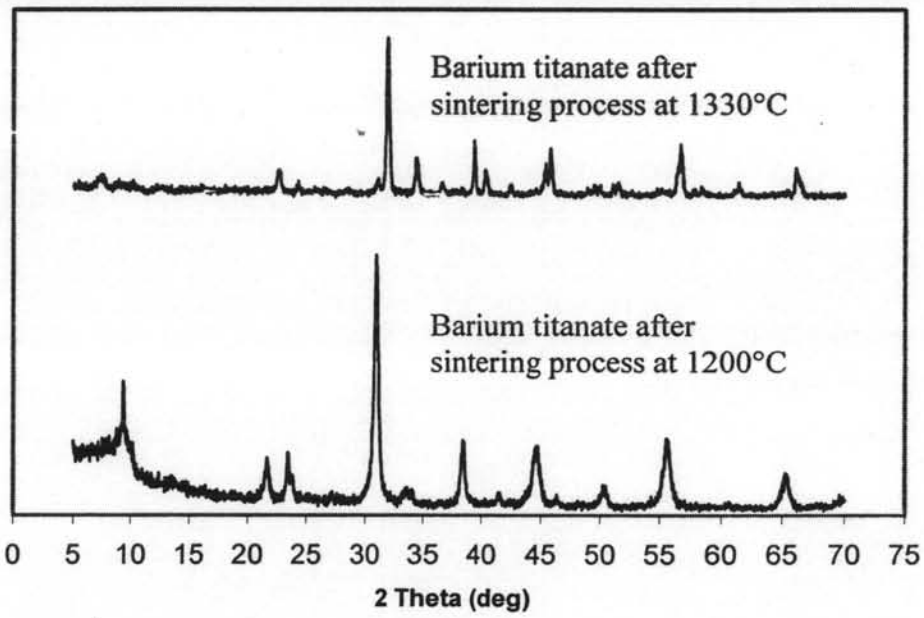

Figure 4.10 XRD spectrum of $BaTiO_3$ after sintering process at 1200°C and 1330°C.

SEM images in Figure 4.11 are consistent with the results of XRD. The microstructures show that small particles are fused together better than in sintering at 1200°C.

(a) 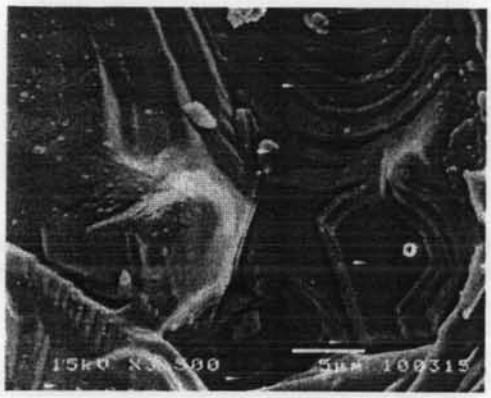 (b) 

Figure 4.11 SEM images of $BaTiO_3$ (a)-and (b) after sintering at 1330°C.

After increasing the temperature of thermal decomposition in the sol-gel process, $(Ba_{0.7}Sr_{0.3})TiO_3$ and $(Ba_{0.5}Sr_{0.5})TiO_3$ are fully crystalline as shown in XRD patterns in Figure 4.12. When increasing the amount of strontium, the temperature of thermal decomposition in the sol-gel process increases because Sr^{2+} ions will occupy the lattice site of the Ba^{2+} ions when strontium is doped into barium titanate,. It will enhance the coupling effect between the Ti^{4+} and O^{2-} ions because the effect of the Sr-O bond is stronger than that of the Ba-O bond. More energy is needed to decompose the compounds, so higher temperature is required (Tian, H.Y et al.). And all major peaks in $(Ba_{0.7}Sr_{0.3})TiO_3$ and $(Ba_{0.5}Sr_{0.5})TiO_3$ XRD patterns are corresponding to the perovskite cubic phase (Yang. X. et al.). And when Sr amount of 0.3 and 0.5 by mole ratio, the perovskite cubic phase was obtained.

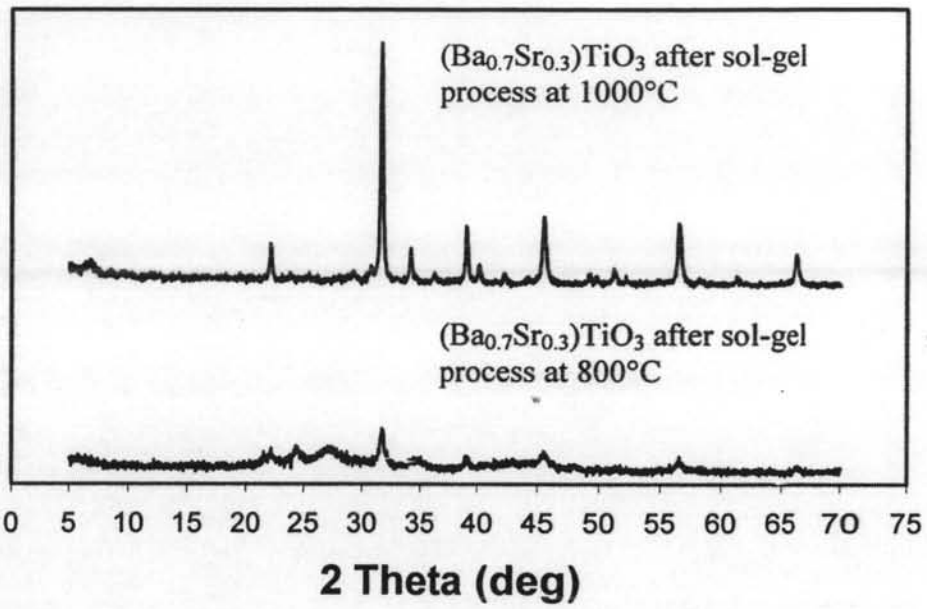

(a)

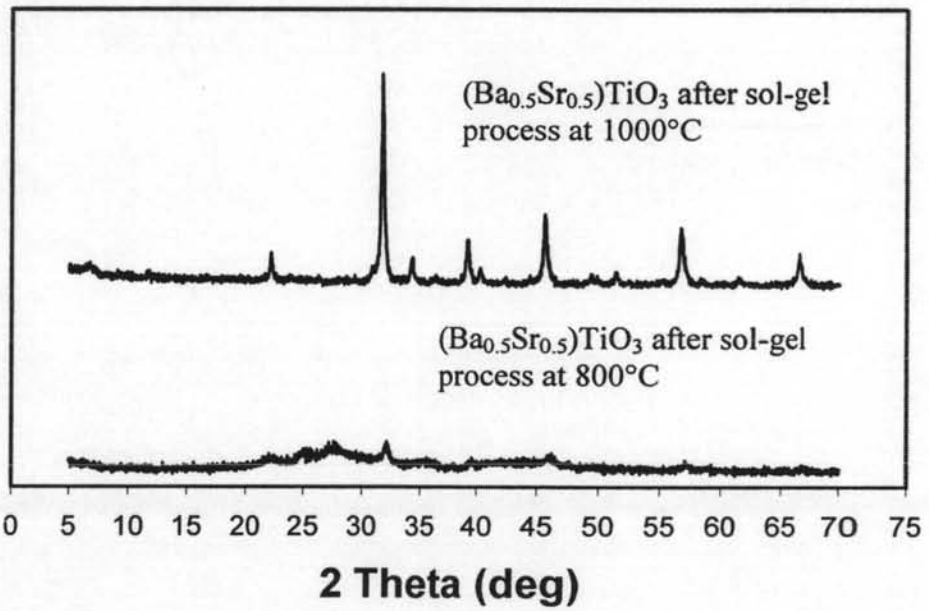

(b)

Figure 4.12 XRD spectrums of Barium strontium titanate after sol-gel process at 800°C and 1000°C (a) $(Ba_{0.7}Sr_{0.3})TiO_3$ (b) $(Ba_{0.5}Sr_{0.5})TiO_3$.

Figures 4.13 and 4.14 show XRD patterns of $(Ba_{0.7}Sr_{0.3})TiO_3$ and $(Ba_{0.5}Sr_{0.5})TiO_3$. Results were similar to $(Ba_{0.95}Sr_{0.05})TiO_3$ in that a higher sintering temperature gave more fully sintered ceramic resulting in higher intensity although the position of peaks are the same. And the sintered ceramic still has the same crystal structure as of after sol-gel process.

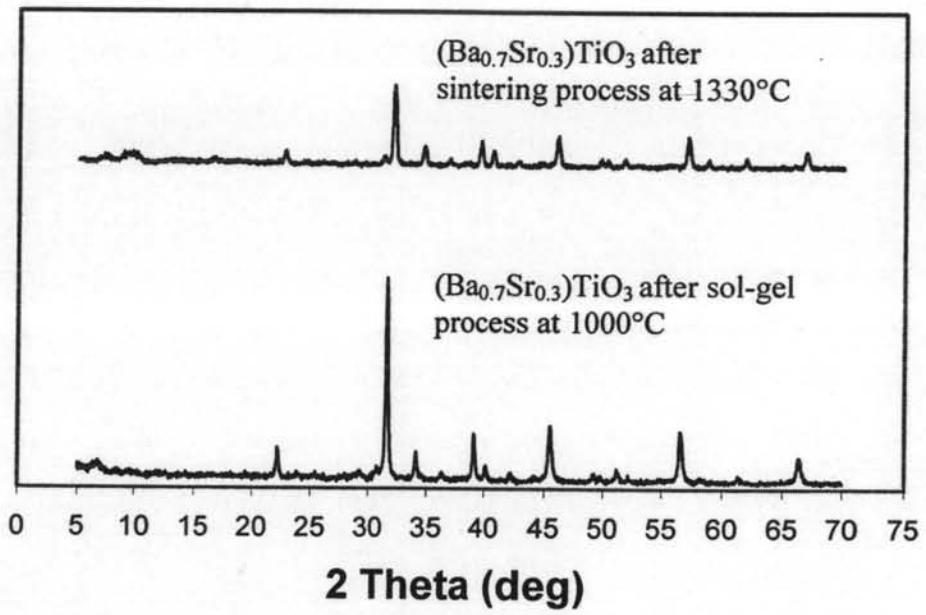

Figure 4.13 XRD spectrum of $(Ba_{0.7}Sr_{0.3})TiO_3$ after sol-gel and sintering process.

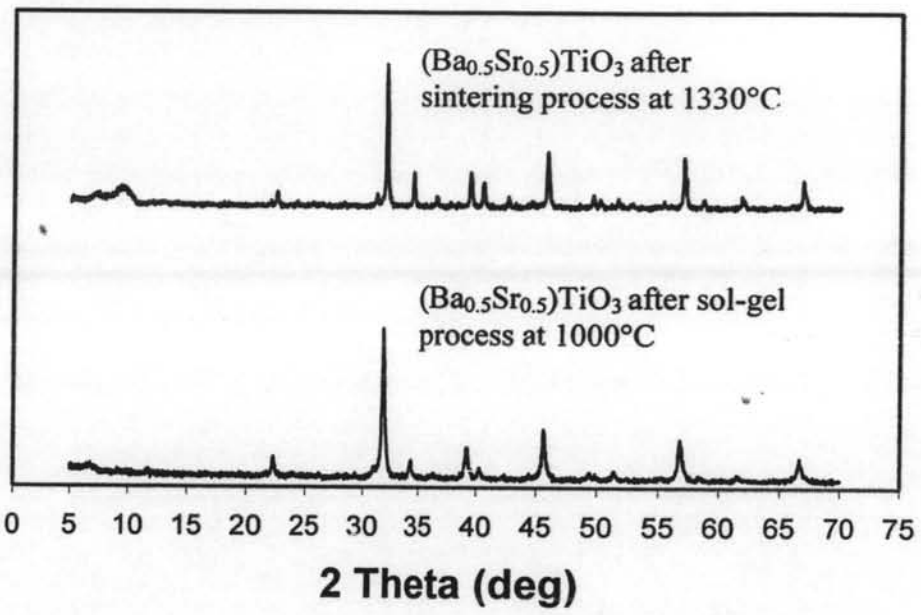

Figure 4.14 XRD spectrum of $(Ba_{0.5}Sr_{0.5})TiO_3$ after sol-gel and sintering process.

Because increasing temperature causes ceramics to be more fully sintered. SEM images in Figures 4.15 and 4.16 of $(Ba_{0.7}Sr_{0.3})TiO_3$ and $(Ba_{0.5}Sr_{0.5})TiO_3$ respectively show microstructures where grain sizes increase as temperatures increases

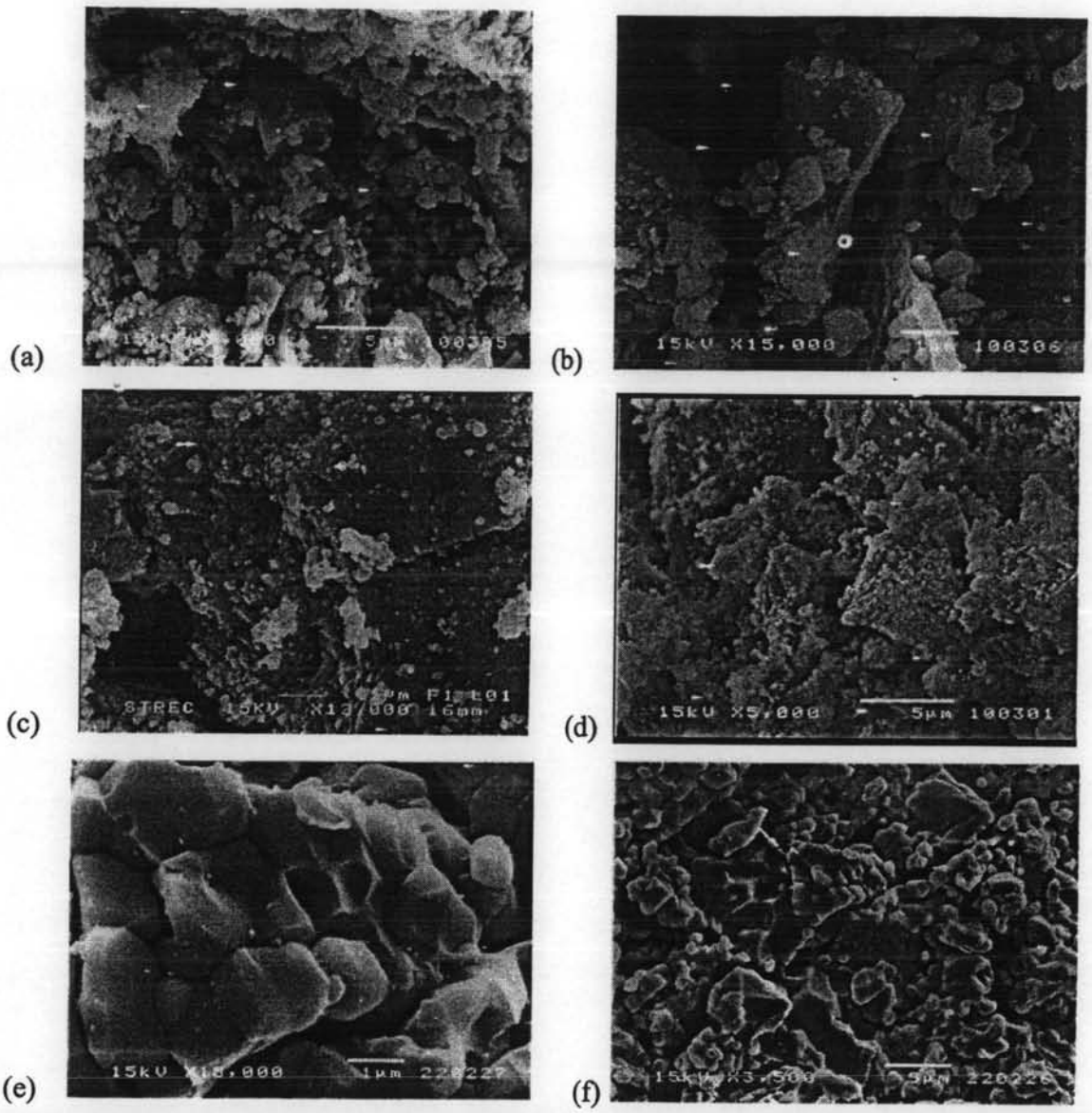

Figure 4.15 SEM images of $(Ba_{0.7}Sr_{0.3})TiO_3$ (a) and (b) after the sol-gel process at 800°C, (c) and (d) after sol-gel process at 1000°C, (e) fracture surface after sintering at 1330°C, and (f) planar surface after sintering at 1330°C.

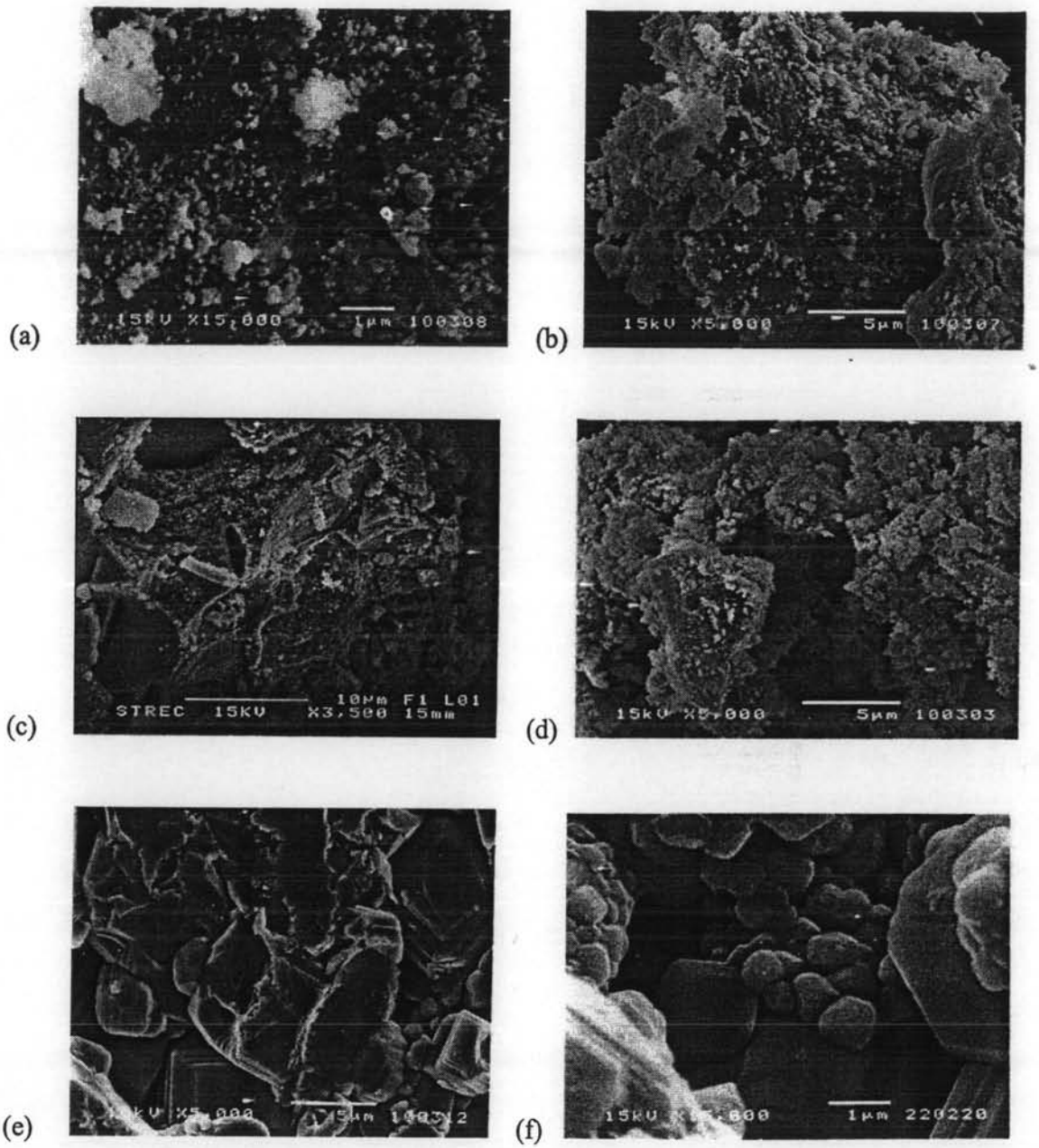

Figure 4.16 SEM images of $(Ba_{0.5}Sr_{0.5})TiO_3$ (a) and (b) after the sol-gel process at 800°C, (c) and (d) after sol-gel process, (e) planar picture after sintering at 1330°C and (f) fracture picture after sintering at 1330°C.

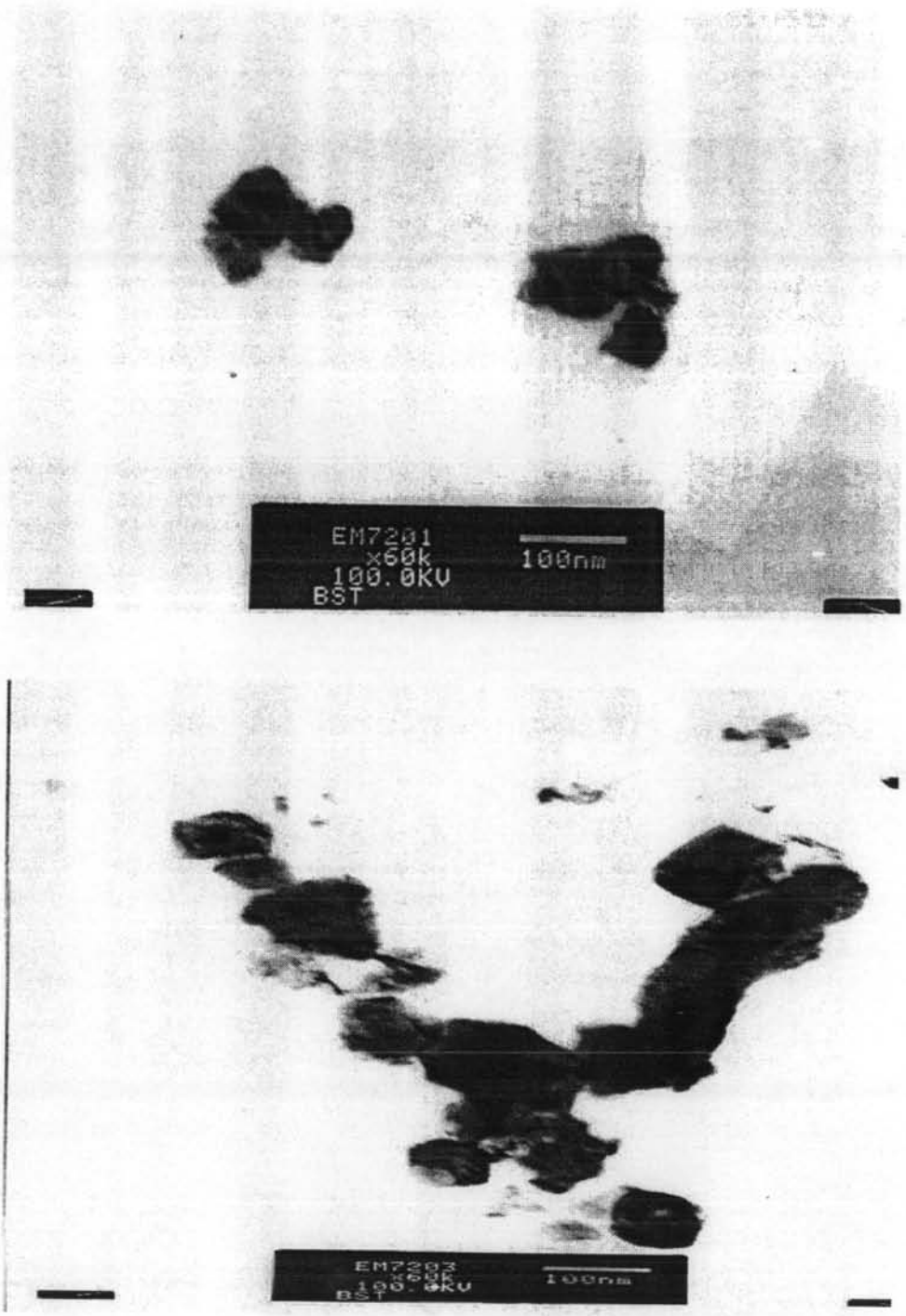

Figure 4.17 TEM images of $(Ba_{0.7}Sr_{0.3})TiO_3$ after sol-gel process at 1000°C.

Since the TEM image in Figure 4.17 shows that the particle size of $(Ba_{0.7}Sr_{0.3})TiO_3$ is in the range of 50 – 80 nm then the particle sizes of another ratio of x in $(Ba_xSr_{1-x})TiO_3$ should be in the same range.

4.3 Thermal Characterization

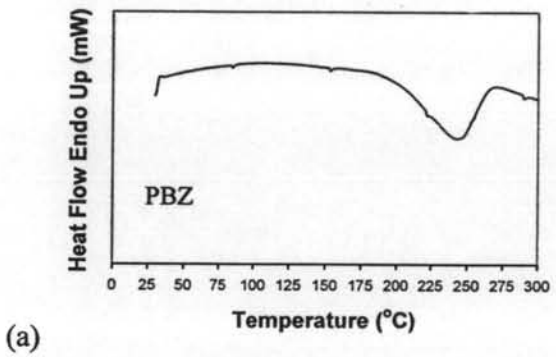

(a)

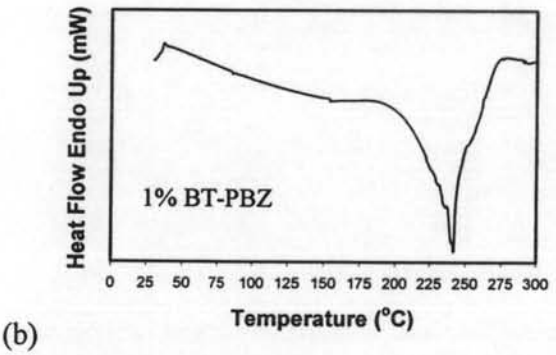

(b)

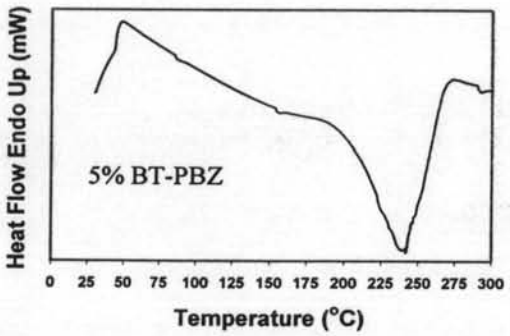

(c)

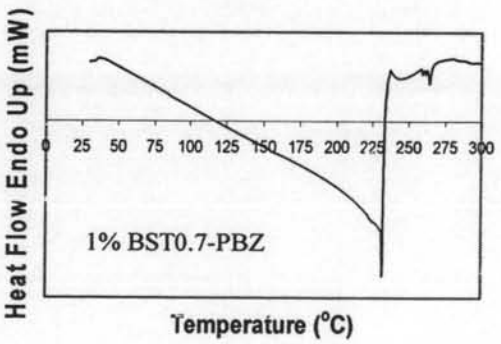

(d)

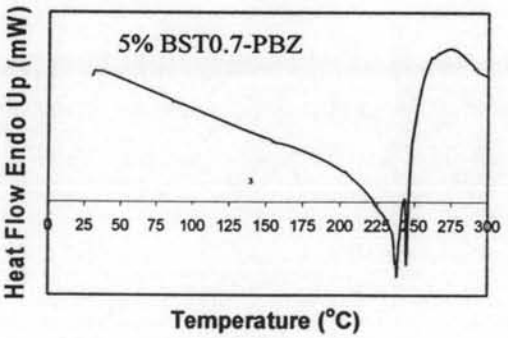

(e)

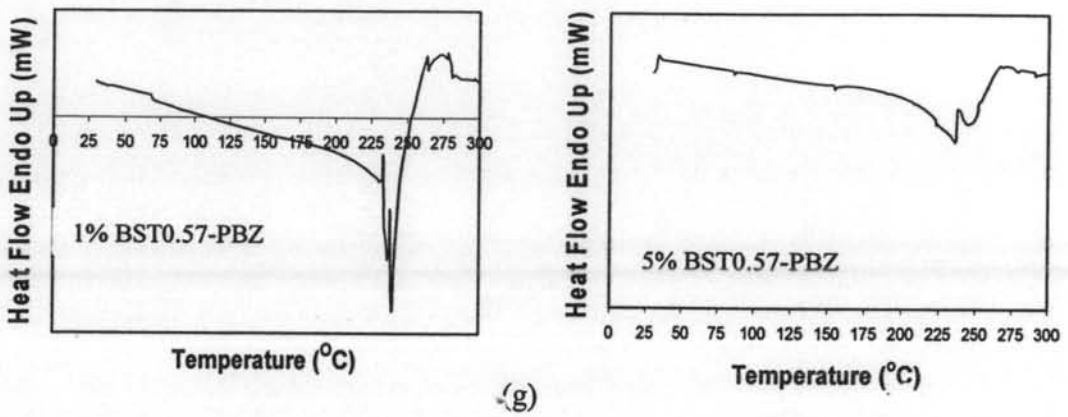

Figure 4.18 DSC thermogram of (a) Polybenzoxazine (PBZ), (b) 1% Barium titanate polybenzoxazine composite (1% BT-PBZ), (c) 5% Barium titanate polybenzoxazine composite (5% BT-PBZ), (d) 1% $(Ba_{0.7}Sr_{0.3})TiO_3$ polybenzoxazine composite (1% BST0.7-PBZ), (e) 5% $(Ba_{0.7}Sr_{0.3})TiO_3$ polybenzoxazine composite (5% BST0.7-PBZ), (f) 1% $(Ba_{0.5}Sr_{0.5})TiO_3$ polybenzoxazine composite (1% BST0.5-PBZ), and (g) 5% $(Ba_{0.5}Sr_{0.5})TiO_3$ polybenzoxazine composite (5% BST0.5-PBZ).

Figure 4.18 shows the DSC thermogram of polybenzoxazine and composites of barium titanate, $(Ba_{0.7}Sr_{0.3})TiO_3$ and $(Ba_{0.7}Sr_{0.3})TiO_3$ in 1% and 5% by weight of composites.

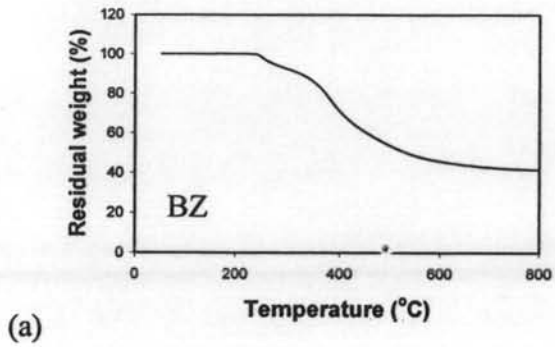
Residual weight (%)
120
100
80
60
40
20
0
BZ
0
200
400
600
800
Temperature (°C)

(a)

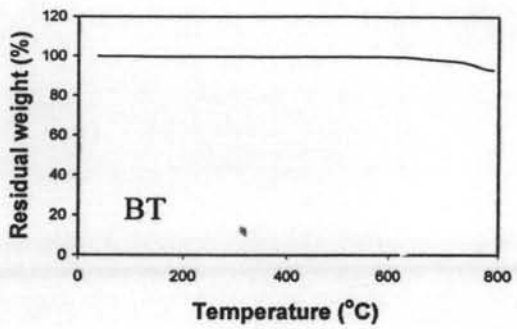
Residual weight (%)
120
100
80
60
40
20
0
BT
0
200
400
600
800
Temperature (°C)

(b)

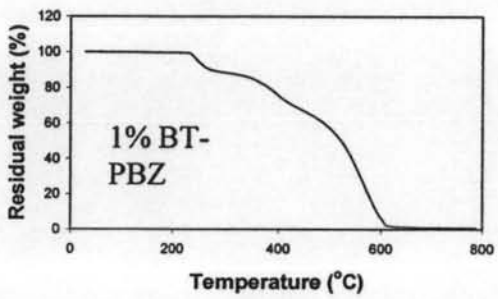
Residual weight (%)
120
100
80
60
40
20
0
1% BT-
PBZ
0
200
400
600
800
Temperature (°C)

(c)

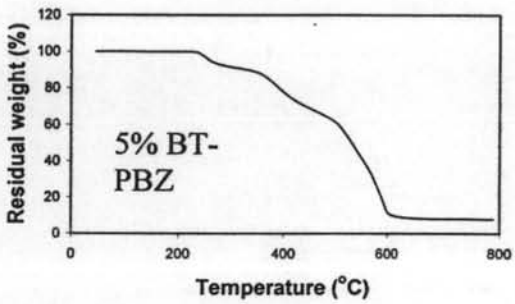
Residual weight (%)
120
100
80
60
40
20
0
5% BT-
PBZ
0
200
400
600
800
Temperature (°C)

(d)

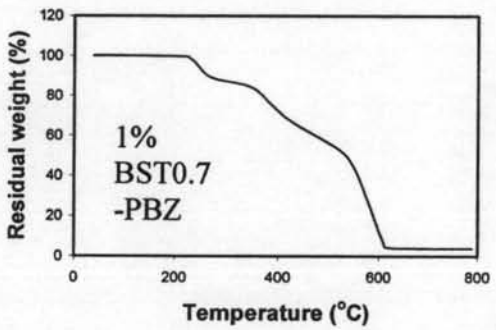
Residual weight (%)
120
100
80
60
40
20
0
1%
BST0.7
-PBZ
0
200
400
600
800
Temperature (°C)

(e)

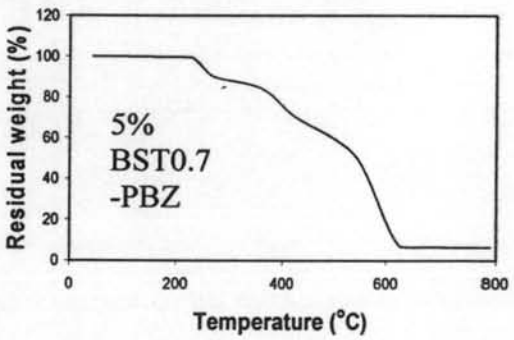
Residual weight (%)
120
100
80
60
40
20
0
5%
BST0.7
-PBZ
0
200
400
600
800
Temperature (°C)

(f)

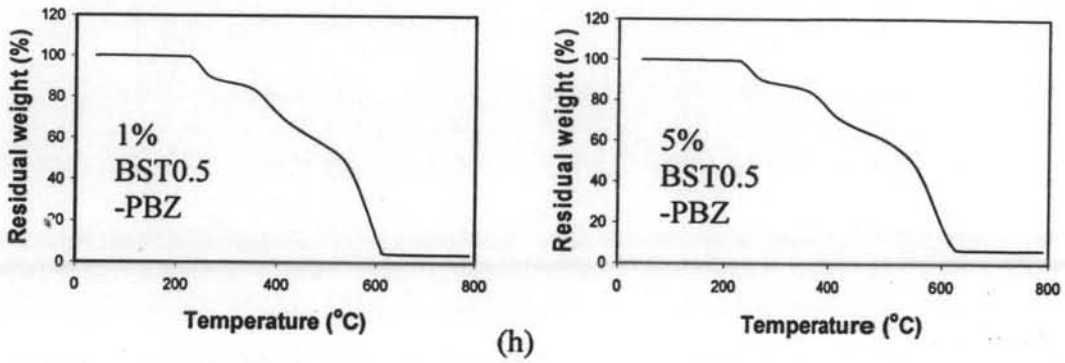

Figure 4.19 TGA thermogram of (a) Benzoxazine monomer (BZ), (b) Barium titanate (BT), (c) 1% Barium titanate polybenzoxazine composite (1% BT-PBZ), (d) 5% Barium titanate polybenzoxazine composite (5% BT-PBZ), (e) 1% $(Ba_{0.7}Sr_{0.3})TiO_3$ polybenzoxazine composite (1% BST0.7-PBZ), (f) 5% $(Ba_{0.7}Sr_{0.3})TiO_3$ polybenzoxazine composite (5% BST0.7-PBZ), (g) 1% $(Ba_{0.5}Sr_{0.5})TiO_3$ polybenzoxazine composite (1% BST0.5-PBZ), and (h) 5% $(Ba_{0.5}Sr_{0.5})TiO_3$ polybenzoxazine composite (5% BST0.5-PBZ).

Figure 4.19 shows the TGA thermogram of polybenzoxazine, barium titanate and composites of barium titanate, $(Ba_{0.7}Sr_{0.3})TiO_3$ and $(Ba_{0.7}Sr_{0.3})TiO_3$ in 1% and 5% by weight of composites. Results show that Monomer started to degrade at 250°C and occurred two steps, polymer composites have more step at 550°C to 600°C may due to the cross linking network of polymer which need more energy to degrade.

4.4 Electrical Measurement

On the addition of strontium titanate, solid solutions retain their ferroelectric nature but the curie point is shifted to lower temperatures linearly with quantity of strontium oxide. By adding of 30 mole% of $SrTiO_3$, the ferroelectric transition takes place near room temperature and its dielectric constant as a function of temperature shows the highest point at room temperature. Figure 4.20 (c), $(Ba_{0.7}Sr_{0.3})TiO_3$ shows a higher dielectric constant when compared to $(Ba_{0.5}Sr_{0.5})TiO_3$) because the ferroelectric transition takes place near room temperature.

Figure 4.20 (a) shows the dielectric constants of various frequencies at 30°C of polybenzoxazine. The dielectric constants are relatively low when compared with those of barium strontium titante and show frequency independence. The dielectric constants of composites (Figure 4.21 to Figure 4.22) are around 8 to 14 because the amounts of ceramic with respect to polymer matrix are relatively low. The reason why the dielectric constant of the polymer-matrix composites remains low at room temperature is because the polymer matrix reduces the overall dielectric constant of the composites. Moreover, the dielectric constant has a weak dependence on frequency and higher concentrations of ferroelectric filler lead to higher dielectric constant composites.

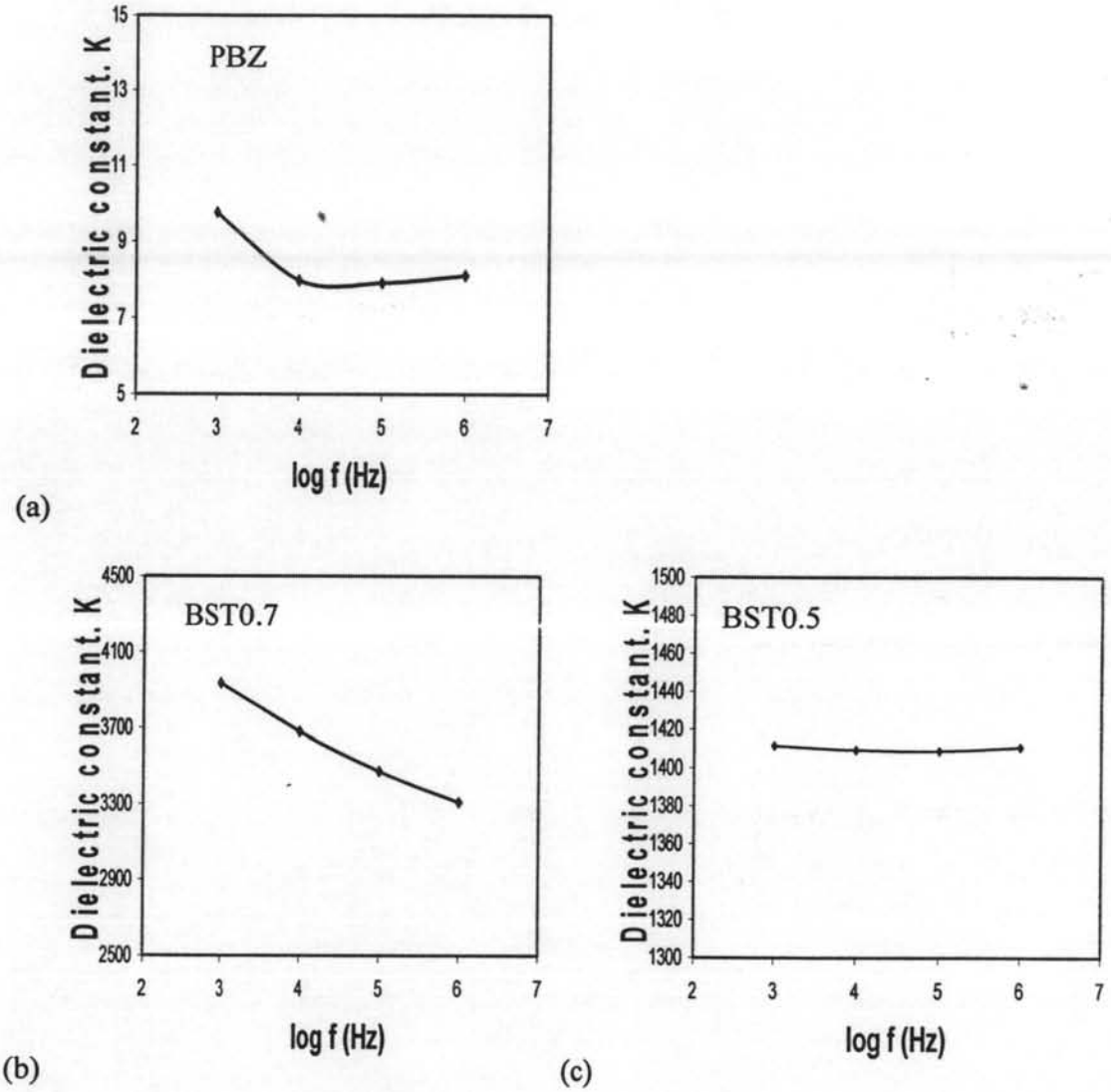

Figure 4.20 Dielectric constant as a function of frequency from 1 kHz to 1 MHz at room temperature of (a) polybenzoxazine (PBZ), (b) $(Ba_{0.7}Sr_{0.3})TiO_3$ (BST0.7), and (c) $(Ba_{0.5}Sr_{0.5})TiO_3$ (BST0.5).

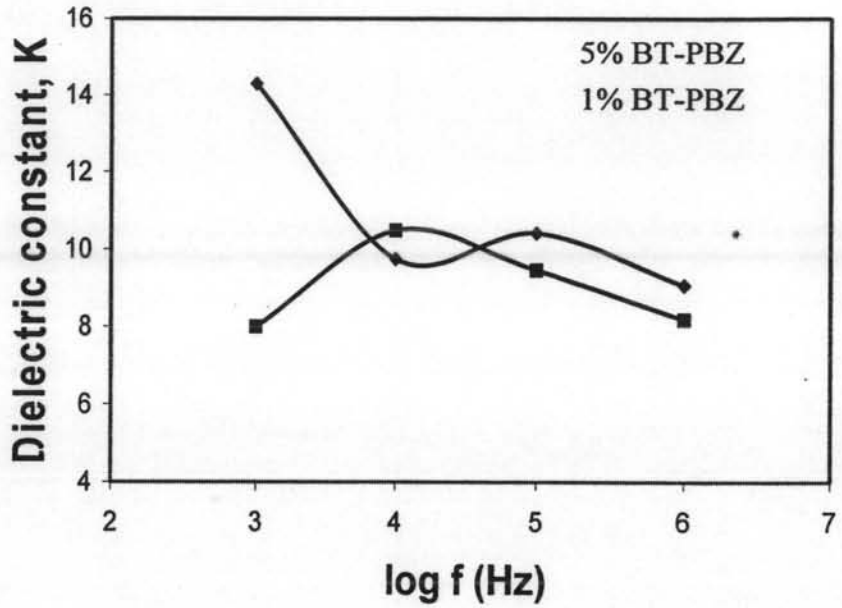

Figure 4.21 Dielectric constant as a function of frequency from 1 kHz to 1 MHz at room temperature of barium titanate benzoxazine composite.

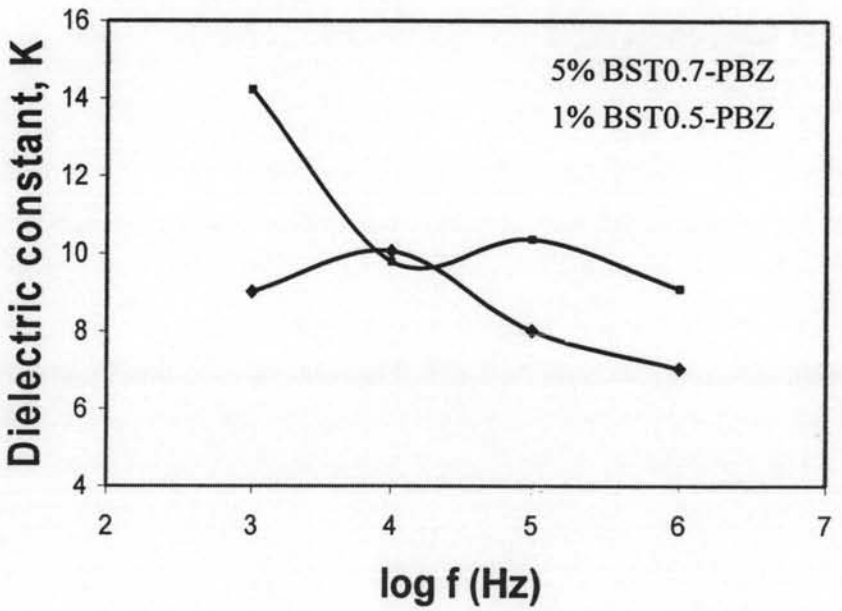

Figure 4.22 Dielectric constant as a function of frequency from 1 kHz to 1 MHz at room temperature of barium strontium titanate $(Ba_{0.7}Sr_{0.3})TiO_3$ benzoxazine composite.

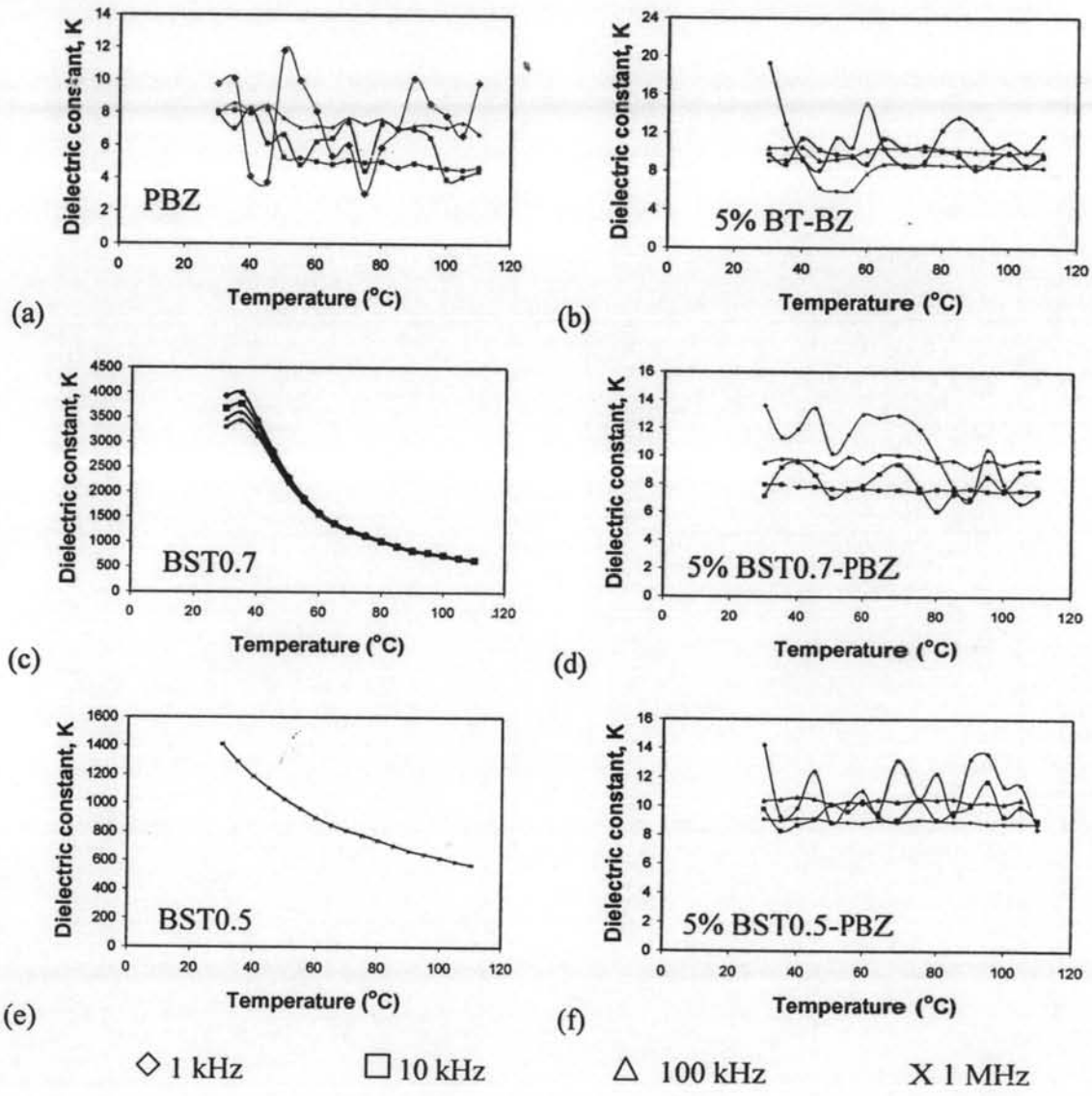

Figure 4.23 Dielectric constant as a function of temperature from 30°C to 110°C of (a) polybenzoxazine (PBZ), (b) 5% barium titanate polybenzoxazine composite (5% BT-PBZ). (c) $(Ba_{0.7}Sr_{0.3})TiO_3$ (BST0.7), (d) 5% $(Ba_{0.7}Sr_{0.3})TiO_3$ polybenzoxazine composite

(5% BST0.7-PBZ), (e) $(Ba_{0.5}Sr_{0.5})TiO_3$ (BST0.5), and (f) 5% $(Ba_{0.5}Sr_{0.5})TiO_3$ polybenzoxazine composite (5% BST0.5-PBZ).

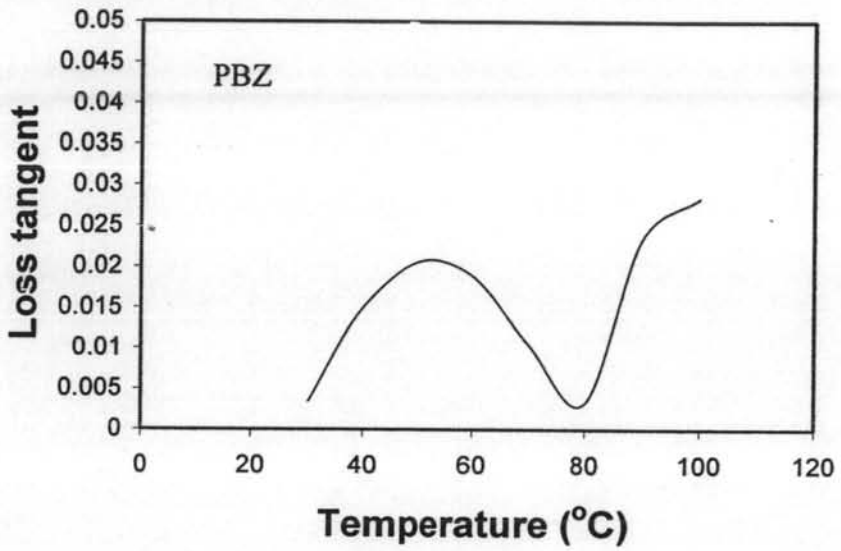

(a)

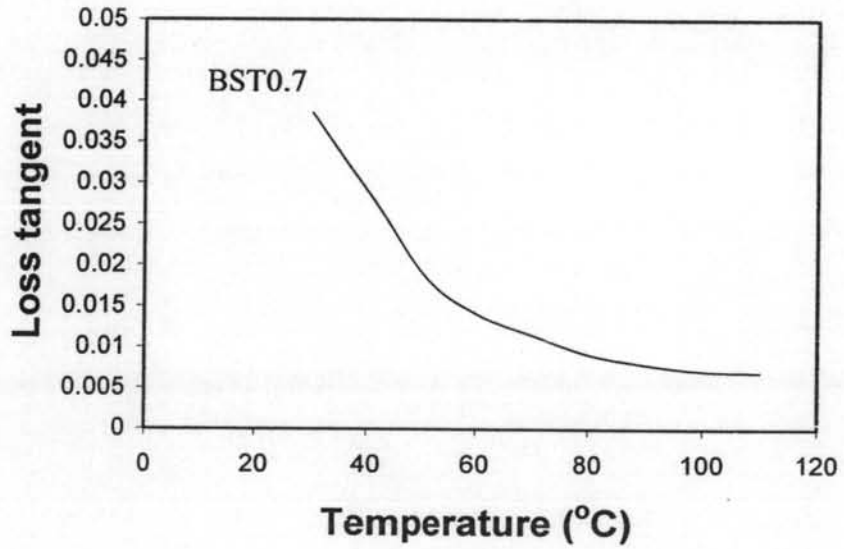

(b)

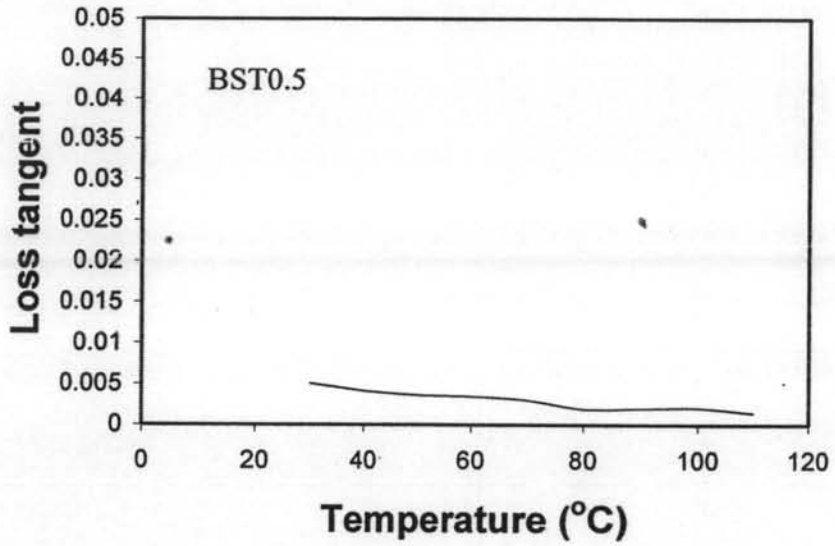
BST0.5
Loss tangent
0.05
0.045
0.04
0.035
0.03
0.025
0.02
0.015
0.01
0.005
0
0
20
40
60
80
100
120
Temperature (°C)

(c)

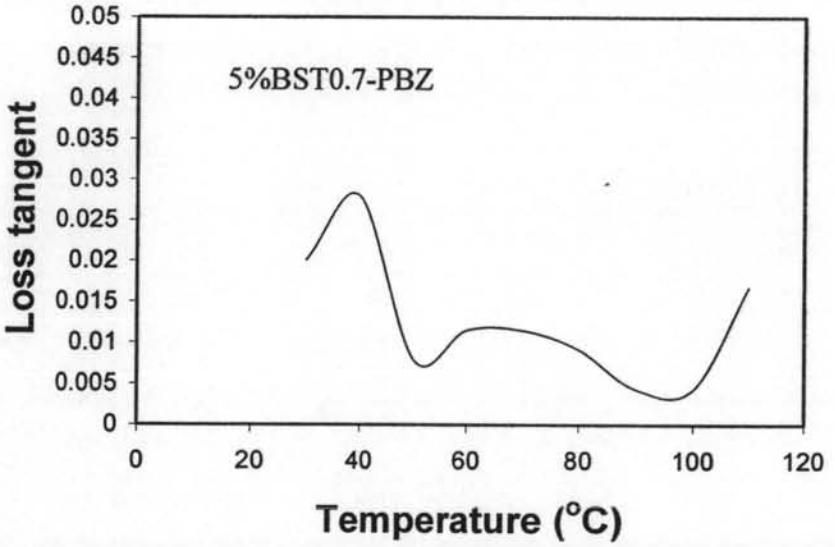
5%BST0.7-PBZ
Loss tangent
0.05
0.045
0.04
0.035
0.03
0.025
0.02
0.015
0.01
0.005
0
0
20
40
60
80
100
120
Temperature (°C)

(d)

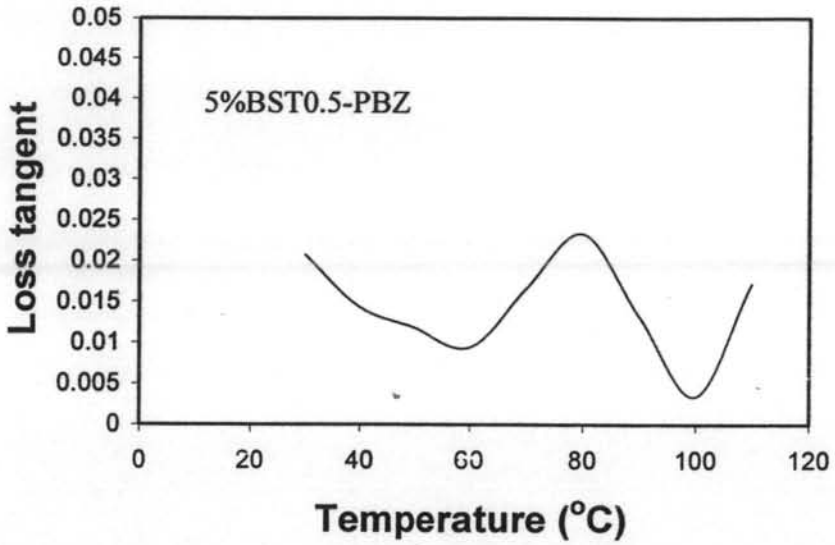

(e)

Figure 4.24 Loss tangent as a function of temperature from 30°C to 110°C of (a) polybenzoxazine (PBZ), (b) $(Ba_{0.7}Sr_{0.3})TiO_3$ (BST0.7), (c) $(Ba_{0.5}Sr_{0.5})TiO_3$ (BST0.5), (d) 5% $(Ba_{0.7}Sr_{0.3})TiO_3$ polybenzoxazine composite (5% BST0.7-PBZ), and (e) 5% $(Ba_{0.5}Sr_{0.5})TiO_3$ polybenzoxazine composite (5% BST0.5-PBZ).

Figure 4.23 shows the effect of temperature on the dielectric properties of nanocomposites $(Ba_{0.7}Sr_{0.3})TiO_3$ and $(Ba_{0.5}Sr_{0.5})TiO_3$ (Figure 4.23 (c) and (d), respectively). All frequencies show that the dielectric constant decreases as temperature increases because $(Ba_{0.7}Sr_{0.3})TiO_3$ has a Curie temperature near room temperature and $(Ba_{0.5}Sr_{0.5})TiO_3$ has a Curie temperature below room temperature. The temperature dependence of the dielectric constant can be described by the generalized Curie law as the dielectric constant of a material decreases after crossing its Curie temperature. Figure 4.23 (a) show the temperature dependence of polybenzoxazine. It was found that at 1 kHz the dielectric constant fluctuates and at higher frequencies the dielectric constant becomes more linear. This was also found in the barium titanate polybenzoxazine composite, $(Ba_{0.7}Sr_{0.3})TiO_3$ polybenzoxazine composite, and $(Ba_{0.5}Sr_{0.5})TiO_3$ polybenzoxazine composite. It means that the dielectric constant of composites strongly depends of the dielectric properties of polymer matrix.

Dielectric losses of the materials were studied and shown in Figure 4.24 The loss tangent (tan δ) of polybenzoxazine is in the range of 0.007 – 0.03, $(Ba_{0.7}Sr_{0.3})TiO_3$ in the range of 0.007 to 0.04, and $(Ba_{0.5}Sr_{0.5})TiO_3$ in the range of 0.001 to 0.005 (Figure 4.25 (a), (b) and (c) respectively).The loss tangent of polybenzoxazine is fluctuation which may be due to a relaxation loss while the loss tangent of measured temperatures (30°C to 110°C) of BST ceramics are low for ceramic characterization. The loss tangent of BST0.7 was higher at 30°C then decreased because this temperature near the Curie temperature which can be seen from dielectric constant experiment. The loss tangents of composites are in the range of 0.005 to 0.03 (Figure 4.24 (d) and (e)) , which shows that dielectric losses of composites depend on both the polymer but does not depend on the ratio of the ceramic components to polymer matrix.